

Exploring the Potential of Low-bit Training of Convolutional Neural Networks

Kai Zhong¹ Xuefei Ning¹ Zhenhua Zhu¹ Tianchen Zhao² Shulin Zeng¹ Yu Wang¹ Huazhong Yang¹

Abstract

In this work, we propose a low-bit training framework for convolutional neural networks, which is built around a novel multi-level scaling (MLS) tensor format. Our framework focuses on reducing the energy consumption of convolution operations by quantizing all the convolution operands to low bit-width format. Specifically, we propose the MLS tensor format, in which the element-wise bit-width can be largely reduced. Then, we describe the dynamic quantization and the low-bit tensor convolution arithmetic to leverage the MLS tensor format efficiently. Experiments show that our framework achieves a superior trade-off between the accuracy and the bit-width than previous low-bit training frameworks. For training a variety of models on CIFAR-10, using 1-bit mantissa and 2-bit exponent is adequate to keep the accuracy loss within 1%. And on larger datasets like ImageNet, using 4-bit mantissa and 2-bit exponent is adequate to keep the accuracy loss within 1%. Through the energy consumption simulation of the computing units, we can estimate that training a variety of models with our framework could achieve $8.3 \sim 10.2\times$ and $1.9 \sim 2.3\times$ higher energy efficiency than training with full-precision and 8-bit floating-point arithmetic, respectively.

1. Introduction

Convolutional neural networks (CNNs) have achieved state-of-the-art performance in many computer vision tasks (Krizhevsky et al., 2012; Redmon et al., 2016; Liu et al., 2016). However, deep CNNs are both computation and storage-intensive. The training process could consume up to hundreds of ExaFLOPs of computations and tens of GBytes of storage (Simonyan & Zisserman, 2014), thus posing a tremendous challenge for training in resource-

Table 1. The number of different operations in the training process on ImageNet (divided by batch size). Abbreviations: “Conv”: convolution; “BN”: batch normalization; “FC”: fully connected layer; “EW-Add”: element-wise addition; “F”: forward; “B”: backward.

| Op Name | Op Type | ResNet18 | GoogleNet |
|----------------|---------|----------|-----------|
| Conv (F) | Mul&Add | 1.88E+09 | 1.58E+09 |
| Conv (B) | Mul&Add | 4.22E+09 | 3.05E+09 |
| BN | Mul&Add | 3.06E+06 | 3.23E+06 |
| FC | Mul&Add | 5.12E+05 | 1.02E+06 |
| EW-Add (F) | Add | 7.53E+05 | 0 |
| EW-Add (B) | Add | 9.28E+05 | 0 |
| SGD Update (B) | Mul&Add | 1.15E+07 | 5.97E+06 |

constrained environments. At present, GPU is commonly used to train CNNs and is energy-consuming. The power of a running GPU is $\sim 250W$, and it usually takes more than 10 GPU-days to train one CNN model on ImageNet (Deng et al., 2009). Therefore, reducing the energy consumption of the training process has raised interest in recent years.

Reducing the precision of CNNs has drawn great attention since it can reduce both the storage and computational complexity. It is pointed out that 32-bit floating-point multiplication and addition units consumes about $20 \sim 30\times$ more power than 8-bit fixed-point ones (Horowitz, 2014). Also, using 8-bit quantization could save the energy consumption of memory access by roughly 4 times. Many studies (Jacob et al., 2018; Banner et al., 2018b; Dong et al., 2019) focus on amending the training process to acquire a reduced-precision model with higher inference efficiency. Besides the studies on improving inference efficiency, there are also some studies that focus on the training process. Wu et al. (2018); Yang et al. (2020) implement fully fixed-point training with 8-bit or 16-bit integers to reduce the cost but fail to get an acceptable accuracy. Wang et al. (2018), Sun et al. (2019) and Cambier et al. (2020) adopt 8-bit floating-point multiplications in convolution. However, the accumulations in their framework are still full-precision, which still account for much energy consumption.

In this work, we design a novel low-bit tensor format with multi-level scaling (MLS format) to improve the energy efficiency of the convolution operations. As shown in Tab. 1, the multiplications and accumulations (MACs) in convolutions are the majority of the operations. Hence, conducting

*Equal contribution ¹Department of Electronic Engineering, Tsinghua University, Beijing, China ²Department of Electronic Engineering, Beihang University, Beijing, China. Correspondence to: Yu Wang <yu-wang@tsinghua.edu.cn>.

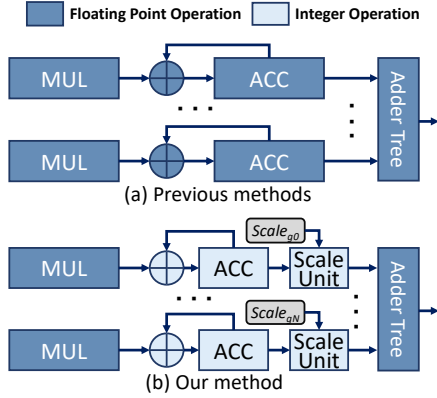


Figure 1. The convolution hardware architecture. (a) Previous studies (Sun et al., 2019) use low-bit floating-point multiplication (FP MUL) (e.g., 8-bit), but FP32 accumulations are still needed. (b) We not only makes MUL less than 8-bit, but also simplifies the local accumulator.

the MACs with low-bit arithmetic in convolutions can boost the energy efficiency of the training process. Specifically, the multi-level scaling technique in the MLS format can largely reduce the element-wise bit-width of the convolution operands without hurting the representational capability. Utilizing the MLS format, our framework conduct multiplications with a smaller bit-width than previous low-bit floating-point frameworks, and the accumulations are conducted with fixed-point arithmetic instead of floating-point arithmetic, as shown in Fig. 1. Therefore, as shown in Fig. 2, our framework can largely reduce the energy consumption of MACs in convolution operations, compared with the full-precision and 8-bit floating-point frameworks. To summarize, the contributions of this paper are:

1. This paper proposes the **MLS tensor format** and the corresponding low-bit training framework to leverage it, in which the core parts are the **dynamic quantization** procedure and the **low-bit tensor convolution arithmetic**. Our framework conducts MACs in convolutions efficiently, without hurting the model accuracy.
2. Experimental results demonstrate the representational capability of the MLS format: For training ResNet, VGG, and GoogleNet on CIFAR-10, using 1-bit mantissa and 2-bit exponent for each element can achieve an accuracy loss within 1%. For training these models on ImageNet, 4-bit mantissa and 2-bit exponent are adequate to achieve an accuracy loss within 1%.
3. We implement Register Transfer Language (RTL) designs of computing units with different arithmetic. And the energy consumption simulation shows that training a variety of models with our framework could

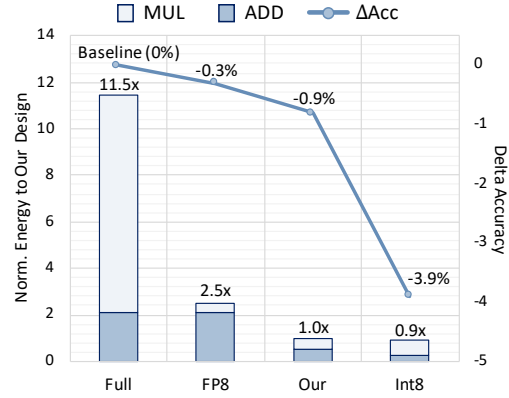


Figure 2. The model accuracy drop (ResNet-18 on ImageNet) and energy consumption of calculating 3×3 convolutions with different training framework, normalized to our design. FP8: (Sun et al., 2019); Int8: (Yang et al., 2020).

achieve $8.3 \sim 10.2\times$ and $1.9 \sim 2.3\times$ higher energy efficiency than training with 32-bit and 8-bit (Sun et al., 2019) floating-point arithmetic. On the other hand, we can achieve much higher accuracy than previous fixed-point training frameworks (Wu et al., 2018; Yang et al., 2020) with comparable energy efficiency.

2. Related work

2.1. Post-Training Quantization

Post-training quantization quantizes a pre-trained full-precision model with various criteria (e.g., SQNR (Lin et al., 2015), entropy (Park et al., 2017)). Banner et al. (2018b); Dong et al. (2019) select the bit-width and clipping value through the analytical investigation. These methods show that low-bit CNN models still have adequate representation ability. However, these methods need a pre-trained model and can not accelerate the training process.

2.2. Quantization-Aware Training

Quantization-aware training considers quantization effects in the training process to further improve the accuracy of the quantized model. It is used for training binary (Rastegari et al., 2016) or ternary (Li et al., 2016) networks. Despite that the follow-up studies (Liu et al., 2020; Qin et al., 2019) have proposed new techniques to improve the accuracy, the extremely low bit-width still causes notable accuracy degradation. Other methods seek to retain the accuracy with relatively higher precision, e.g., 8-bit (Jacob et al., 2018). Gysel et al. (2018) develop GPU-based training framework to get dynamic fixed-point models. These methods obtain quantized models for more efficient inference, but the train-

ing process is still full-precision.

2.3. Low-Bit Training

To accelerate the training process, Zhou et al. (2016) propose to use fixed-point arithmetic in both forward and backward processes. Wu et al. (2018); Yang et al. (2020) implement full-integer training frameworks for integer-arithmetic machines. However, these methods cause notable accuracy degradation. Banner et al. (2018a) use 8-bit and 16-bit integer arithmetic (Jacob et al., 2017) and achieve a better accuracy. But this arithmetic (Jacob et al., 2017) is designed for accelerating inference and requires knowing the output scale before calculation. Therefore, although Banner et al. (2018a) quantize the gradients in the backward process, it is not practical for actual training acceleration.

Besides the studies on full-integer training frameworks, some studies propose new low-bit formats. Abadi et al. (2016) use a 16-bit floating-point format that is more suitable for CNN training. Köster et al. (2017) propose the Flexpoint format that contains 16-bit mantissa and 5-bit tensor-shared exponent (scale), which is similar to the dynamic fixed-point format proposed by Das et al. (2018). Recently, 8-bit floating-point formats (Wang et al., 2018; Sun et al., 2019; Cambier et al., 2020) are used with chunk-based accumulation and hybrid format. However, the exponent bit-width in their format is still as large as 5, which makes the operations using this format (especially the accumulation) very inefficient. In this work, the MLS tensor format is designed to have a small exponent bit-width, such that the accumulation can be conducted using fixed-point arithmetic.

3. Multilevel Scaling Low-bit Tensor Format

In this section, we introduce the MLS low-bit tensor format, which is the core of our low-bit training framework. We denote the filter and feature map of convolutions as weight and activation, and the gradients of feature map and weights are denoted as error and gradient, respectively. And all these tensors are 4-dimension tensors in the training process.

3.1. Mapping Formula of the MLS Format

In a commonly used scheme (Jacob et al., 2017), the mapping function from fixed-point representation and the floating-point values is $float = scale \times (Fix + Bias)$, in which $scale$ and $Bias$ are shared in one tensor. However, since data distribution changes over time, one cannot simplify the $Bias$ calculation as Jacob et al. (2017) did in training. Thus, we adopt an unbiased quantization scheme, and extend the scaling factor to three levels for better representation ability. The resulting MLS tensor format is illustrated in Fig. 3. Denoting a 4-dimensional tensor that is the operand of Conv (weight, activation, or error) as \mathbf{X} , the

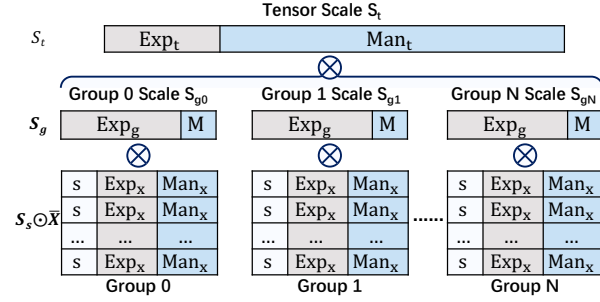


Figure 3. The multi-level scaling (MLS) low-bit tensor format.

mapping formula of the MLS tensor format is

$$\mathbf{X}[i, j, k, l] = \mathbf{S}_s[i, j, k, l] \times S_t \times \mathbf{S}_g[i, j] \times \bar{\mathbf{X}}[i, j, k, l] \quad (1)$$

where $[\cdot]$ denotes the indexing operation, \mathbf{S}_s is a 1-bit sign tensor ("s" in Fig. 3), S_t is a full-precision tensor-wise scaling factor, and \mathbf{S}_g are group-wise scaling factors shared in each group. \mathbf{S}_g and $\bar{\mathbf{X}}$ use the same data format, which we refer to as $\langle E, M \rangle$, a customized floating-point format with E-bit exponent and M-bit mantissa (no sign bit). A value in the format $\langle E, M \rangle$ is

$$\begin{aligned} float &= I2F(Man, Exp) = \text{Frac} \times 2^{-Exp} \\ &= \left(1 + \frac{Man}{2^M}\right) \times 2^{-Exp} \end{aligned} \quad (2)$$

where Man and Exp are the M-bit mantissa and E-bit exponent, and $\text{Frac} \in [1, 2)$ is a fraction.

Our work considers three grouping dimensions: 1) grouping by the 1-st dimension of tensor, 2) the 2-nd dimension of tensor, or 3) the 1-st and the 2-nd dimensions simultaneously. Group-wise scaling is beneficial because the data ranges vary across different groups, as shown in Fig. 4. The blue line shows the max value in each group when activation and error are grouped by channel or sample. If we use the overall maximum value (green lines in Fig. 4) as the overall scaling, many small elements will be swamped. And usually, there are over half of the groups, in which all elements are smaller than half of the overall maximum (red line). Thus, to fully exploit the bit-width, it is natural to use group-wise scaling factors. And by using both the tensor-wise and group-wise scaling factors, the bit-width of $\bar{\mathbf{X}}$ can be largely reduced.

3.2. Details on the Scaling Factors

The first level **tensor-wise scaling factor** S_t is an ordinary floating-point number to retain the precision as much as possible. Considering the actual hardware implementation cost, there are some restrictions on the second level **group-wise scaling factor** \mathbf{S}_g . Since calculation results of

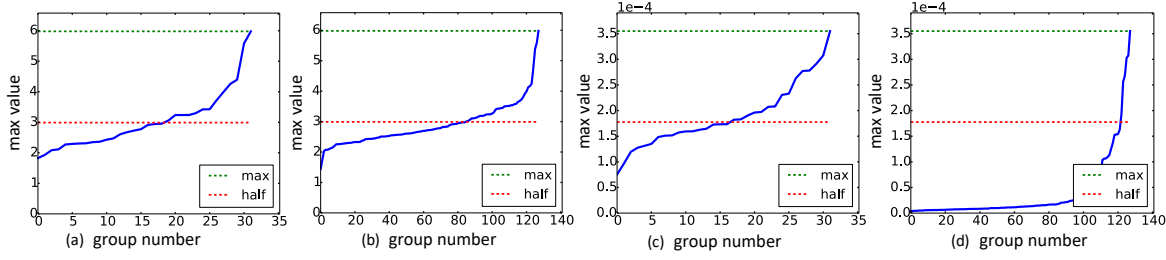


Figure 4. Maximum value of each group of activation (a, b) and error (c, d). (a)(c): Grouped by channel; (b)(d): Grouped by sample.

different groups need to be aggregated, using S_g in an ordinary floating-point format leads to expensive conversions in the hardware implementation. So we propose two special hardware-friendly group-wise scaling schemes, whose formats can be denoted as $\langle E_g, 0 \rangle$, and $\langle E_g, 1 \rangle$, respectively. The scaling factor in $\langle E_g, 0 \rangle$ format is simply a power of two, which can be implemented easily as shifting on the hardware. From Eq. 2, a $S_g = I2F(Man_g, Exp_g)$ value in the $\langle E_g, 1 \rangle$ format can be written as

$$S_g = \left(1 + \frac{Man_g}{2}\right) \times 2^{-Exp_g} = \begin{cases} 2^{-Exp_g} + 2^{-Exp_g-1} & Man_g = 1 \\ 2^{-Exp_g} & Man_g = 0 \end{cases} \quad (3)$$

which is a sum of two shifting, and can also be implemented with low hardware overhead. We will see that MLS tensor convolution arithmetic benefits from group-wise scaling factor's special format with very few mantissa bits in Sec. 4.2 (Eq. 8). The third level scaling factor $S_x = I2F(0, Exp_x) = 2^{-Exp_x}$ is the **element-wise exponent** in $\tilde{X} = S_x(1 + \frac{Man_x}{2})$, and we can see that the elements of \tilde{X} in Eq. 1 are in a $\langle E_x, M_x \rangle$ format. The specific values of E_x and M_x determine the cost of the MAC operation, which will be discussed in Sec. 4.2.

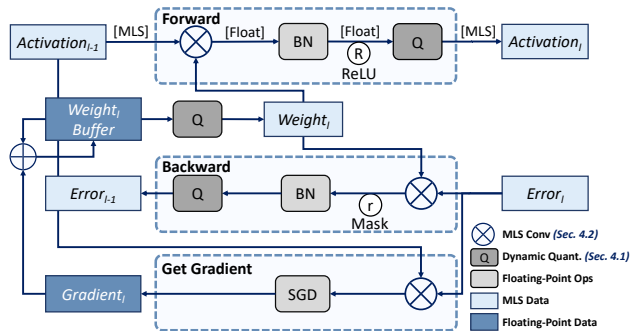


Figure 5. Computation flow of our low-bit training framework.

4. Low-bit Training Framework of CNN

In this section, we describe the low-bit training framework to leverage the MLS tensor format. The overall low-bit training framework is shown in Fig. 5. Since convolution accounts for the majority computational cost, we apply quantization before all convolutions in the training process, including three types: Conv(Weight, Activation), Conv(Weight, Error), and Conv(Activation, Error). Note that, this framework is different from a quantization-aware training framework in that the convolution operands are actually quantized to the low-bit MLS format in our computation flow. And the output data of Conv is in floating-point format, and other operations operate on floating-point numbers.

We summarize a training iteration in our framework as an algorithm in the appendix, and describe two core parts of the framework in this section, i.e., the dynamic quantization *DynamicQuantization* (Sec. 4.1) and the low-bit tensor convolution arithmetic *LowbitConv* (Sec. 4.2).

4.1. Dynamic Quantization to MLS Tensor

The dynamic quantization converts a floating-point tensor to a MLS tensor by calculating the scaling factors S_s, S_t, S_g and getting the quantized elements \tilde{X} , as shown in Alg. 1. In Alg. 1, *Exponent*(\cdot) and *Fraction*(\cdot) are to obtain the Exponent (an integer) and Fraction (an integer $\in [1, 2)$) of a floating-point number. And the underflow handling follows the IEEE 754 standard (Hough, 2019). When calculating the quantized elements \tilde{X} , we apply the stochastic rounding (Gupta et al., 2015) *SRound*(x, r). It is implemented with a uniformly distributed random tensor $r \sim U[-0.5, 0.5]$.

$$SRound(x, r) = NearestRound(x + r) = \begin{cases} \lfloor x \rfloor & \text{with probability } x - \lfloor x \rfloor \\ \lceil x \rceil & \text{with probability } \lceil x \rceil - x \end{cases} \quad (4)$$

Note that Alg. 1 describes how we simulate the dynamic quantization process on floating-point platform. While in the hardware design, the exponent and mantissa are obtained

Algorithm 1 Dynamic Quantization

Input: \mathbf{X} : float 4-d tensor; \mathbf{R} : $U[-\frac{1}{2}, \frac{1}{2}]$ distributed random tensor; $\langle E_g, M_g \rangle$: bit-width of group-wise scaling factors; $\langle E_x, M_x \rangle$: bit-width of each element

Output: \mathbf{S}_s : sign tensor; \mathbf{S}_t : tensor-wise scaling factor; \mathbf{S}_g : group-wise scaling factors; $\bar{\mathbf{X}}$: quantized elements

// calculating scaling factors

```

1  $\mathbf{S}_s = \text{Sign}(\mathbf{X})$ 
2  $\mathbf{S}_r = \text{GroupMax}(\text{Abs}(\mathbf{X}))$ 
3  $\mathbf{S}_t = \text{Max}(\mathbf{S}_r)$ 
4  $\mathbf{S}_{gf} = \mathbf{S}_r \div \mathbf{S}_t$ 
5  $\text{Exp}_g, \text{Frac}_g = \text{Exponent}(\mathbf{S}_{gf}), \text{Fraction}(\mathbf{S}_{gf})$ 
6  $\text{Exp}_g = \text{Clip}(\text{Exp}_g, 1 - 2^{E_g}, 0)$ 
7  $\text{Frac}_g = \text{Ceil}(\text{Frac}_g \times 2^{M_g}) \div 2^{M_g}$ 
8  $\mathbf{S}_g = \text{Frac}_g \times 2^{\text{Exp}_g}$ 

```

// calculating elements

```

9  $\mathbf{X}_f = \text{Abs}(\mathbf{X}) \div \mathbf{S}_g \div \mathbf{S}_t$ 
10  $\text{Exp}_x, \text{Frac}_x = \text{Exponent}(\mathbf{X}_f), \text{Fraction}(\mathbf{X}_f)$ 

```

// quantize Frac_x to M_x bits with underflow handling

```

11  $E_{x\min} = 1 - 2^{E_x}$ 
12  $\text{Frac}_{xs} = \text{Frac}_x \times 2^{M_x}$  if not underflow, else  $\text{Frac}_x \times 2^{M_x - E_{x\min} + E_x}$ 
13  $\text{Frac}_{xint} = \text{Clip}(\text{SRound}(\text{Frac}_{xs}, \mathbf{R}), 0, 2^{M_x} - 1)$ 
14  $\text{Frac}_x = \text{Frac}_{xint} \times 2^{-M_x}$  if not underflow, else  $\text{Frac}_{xint} \times 2^{-M_x + E_{x\min} - E_x}$ 
15  $\text{Exp}_x = \text{Clip}(\text{Exp}_x, E_{x\min}, -1)$ 
16  $\bar{\mathbf{X}} = \text{Frac}_x \times 2^{\text{Exp}_x}$ 
Return  $\mathbf{S}_s, \mathbf{S}_t, \mathbf{S}_g, \bar{\mathbf{X}}$ 

```

directly, while the *Clip* operations are conducted by taking out some bits from a machine number.

4.2. Low-bit Tensor Convolution Arithmetic

In this section, we describe how to do convolution with two low-bit MLS tensors. We take $\text{Conv}(\text{Weight}, \text{Activation})$ ($\text{Conv}(\mathbf{W}, \mathbf{A})$) as the example, and the other two types of convolution can be implemented similarly. Denoting the input channel number as C and the kernel size as K , the original formula of convolution is:

$$\mathbf{Z}[n, co, x, y] = \sum_{ci=0}^{C-1} \sum_{i=0}^{K-1} \sum_{j=0}^{K-1} \mathbf{W}[co, ci, i, j] \times \mathbf{A}[n, ci, x+i, y+j] \quad (5)$$

Using the MLS tensor format and denoting the corresponding values (scaling factors \mathbf{S} , exponents Exp and fractions Frac in the following equations) of \mathbf{W} and \mathbf{A} by the superscript (w) and (a) , one output element $\mathbf{Z}[n, co, x, y]$ of

$\text{Conv}(\mathbf{W}, \mathbf{A})$ is calculated as:

$$\begin{aligned} \mathbf{Z}[n, co, x, y] &= \sum_{ci=0}^{C-1} \sum_{i=0}^{K-1} \sum_{j=0}^{K-1} \left(S_t^{(w)} S_g^{(w)}[co, ci] \bar{\mathbf{W}}[co, ci, i, j] \right) \\ &\quad \left(S_t^{(a)} S_g^{(a)}[n, ci] \bar{\mathbf{A}}[n, ci, x+i, y+j] \right) \\ &= \left(S_t^{(w)} S_t^{(a)} \right) \sum_{ci=0}^{C-1} \left[\left(S_g^{(w)}[co, ci] S_g^{(a)}[n, ci] \right) \right. \\ &\quad \left. \sum_{i=0}^{K-1} \sum_{j=0}^{K-1} \bar{\mathbf{W}}[co, ci, i, j] \bar{\mathbf{A}}[n, ci, x+i, y+j] \right] \\ &= S_t^{(z)} \sum_{ci=0}^{C-1} \mathbf{S}^{(p)}[n, co, ci] \mathbf{P}[n, co, ci] \end{aligned} \quad (6)$$

Eq. 6 shows that the accumulation consist of **intra-group** MACs that calculates $\mathbf{P}[n, co, ci]$ and **inter-group** MACs that calculates \mathbf{Z} .

Intra-group MACs The intra-group calculation of $\mathbf{P}[n, co, ci]$ is:

$$\begin{aligned} \mathbf{P}[n, co, ci] &= \sum_{i,j=0}^{K-1} \left(\text{Frac}^{(w)}[co, ci, i, j] \text{Frac}^{(a)}[n, ci, i, j] \right) \\ &\quad \times 2^{\left(\text{Exp}^{(w)}[co, ci, i, j] + \text{Exp}^{(a)}[n, ci, i, j] \right)} \end{aligned} \quad (7)$$

where Frac , Exp are $(M_x + 1)$ -bit and E_x -bit. Thus the intra-group calculation contains the multiplication of two $(M_x + 1)$ -bit values and $2 \times (2^{E_x} - 2)$ -bit shifting. The resulting $(2M_x + 2^{E_x+1} - 2)$ -bit¹ integer values need to be accumulated with enough bit-width to get the partial sum \mathbf{P} . In previous 8-bit floating-point frameworks (Wang et al., 2018; Sun et al., 2019), the accumulator has to be floating-point since they use $E_x = 5$. In contrast, we can use a 32-bit integer accumulator, since we adopt $E_x = 2$, $M_x = 4$ in the MLS tensor format on ImageNet.

Inter-group MACs As for the inter-group calculation, each element in $\mathbf{S}^{(p)}$ is a $\langle E, 2 \rangle$ number obtained by multiplying two $\langle E, 1 \rangle$ numbers. So it can be calculated by shift (multiplying the power of two) and addition as:

$$\begin{aligned} \mathbf{Z}[co, x] &= S_t^{(z)} \sum_{ci=0}^{C-1} \mathbf{S}^{(p)}[co, ci] \mathbf{P}[x, ci] = S_t^{(z)} \sum_{ci=0}^{C-1} \\ &\quad \begin{cases} \mathbf{P}[x, ci] 2^{-\text{Exp}^{(p)}[co, ci]} \\ \mathbf{P}[x, ci] 2^{-\text{Exp}^{(p)}[co, ci]} + \mathbf{P}[x, ci] 2^{-\text{Exp}^{(p)}[co, ci]-1} \\ \mathbf{P}[x, ci] 2^{1-\text{Exp}^{(p)}[co, ci]} + \mathbf{P}[x, ci] 2^{-\text{Exp}^{(p)}[co, ci]-2} \end{cases} \end{aligned} \quad (8)$$

where the three cases correspond to $\text{Man}^{(p)}[co, ci]=00$, $\text{Man}^{(p)}[co, ci]=01/10$, and $\text{Man}^{(p)}[co, ci]=11$, respec-

¹The derivation is shown in the appendix.

Table 2. Comparison of low-bit training methods on CIFAR-10 and ImageNet. Single number in the bit-width stands for fixed-point format bit-width, which is equivalent to M_x and the corresponding E_x is 0. “f x” indicates that x-bit floating-point numbers are used. “ACC” in the “Bit-Width” column stands for “Accumulation”, while “Acc.” stands for “Accuracy”.

| Dataset | Method | Model | Bit-Width (W/A/E/ACC) | Acc. | FP baseline | Acc. Drop |
|----------|------------------------|-----------|--|-------------|-------------|-----------|
| CIFAR-10 | (Cambier et al., 2020) | ResNet-20 | $\langle 5, 2 \rangle \langle 5, 2 \rangle \langle 5, 2 \rangle$ f32 | 91.1% | 91.5% | 0.4% |
| | (Wu et al., 2018) | VGG-like | 2 8 8 32 | 93.2% | 94.1% | 0.9% |
| | (Banner et al., 2018a) | ResNet-20 | 1 1 2 - | 81.5% | 90.36% | 8.86% |
| | Ours | ResNet-20 | 4 4 4 16 | 92.32% | 92.45% | 0.13% |
| | | ResNet-20 | 2 2 2 16 | 90.39% | 92.45% | 2.06% |
| | | ResNet-20 | $\langle 2, 1 \rangle \langle 2, 1 \rangle \langle 2, 1 \rangle$ 16 | 91.97% | 92.45% | 0.48% |
| | | GoogleNet | $\langle 2, 1 \rangle \langle 2, 1 \rangle \langle 2, 1 \rangle$ 16 | 93.95% | 94.50% | 0.55% |
| | | VGG-16 | $\langle 2, 1 \rangle \langle 2, 1 \rangle \langle 2, 1 \rangle$ 16 | 93.34% | 93.76% | 0.42% |
| | | VGG-16 | $\langle 1, 1 \rangle \langle 1, 1 \rangle \langle 1, 1 \rangle$ 8 | 92.77% | 93.76% | 0.99% |
| ImageNet | (Köster et al., 2017) | AlexNet | 16 16 16 32 | 80.1%(Top5) | 79.9%(Top5) | -0.2% |
| | (Das et al., 2018) | VGG-16 | 16 16 16 32 | 68.2% | 68.1% | -0.1% |
| | (Das et al., 2018) | GoogleNet | 16 16 16 32 | 69.3% | 69.3% | 0 |
| | (Banner et al., 2018a) | ResNet-18 | 8 8 16 f32 | 66.4% | 67.0% | 0.6% |
| | (Zhou et al., 2016) | AlexNet | 8 8 8 32 | 53.0% | 55.9% | 2.9% |
| | (Yang et al., 2020) | ResNet-18 | 8 8 8 32 | 64.8% | 68.7% | 3.9% |
| | (Yang et al., 2020) | ResNet-34 | 8 8 8 32 | 67.6% | 72.0% | 4.4% |
| | (Wu et al., 2018) | AlexNet | 2 8 8 32 | 48.4% | 56.0% | 7.6% |
| | (Sun et al., 2019) | ResNet-18 | $\langle 5, 3 \rangle \langle 5, 3 \rangle \langle 5, 3 \rangle$ f32 | 69.0% | 69.3% | 0.3% |
| | (Cambier et al., 2020) | ResNet-18 | $\langle 5, 2 \rangle \langle 5, 2 \rangle \langle 5, 2 \rangle$ f32 | 69.6% | 70.3% | 0.7% |
| | Ours | ResNet-18 | 8 8 8 32 | 68.5% | 69.1% | 0.6% |
| | | ResNet-18 | 4 4 4 16 | 66.5% | 69.1% | 2.6% |
| | | ResNet-18 | $\langle 2, 4 \rangle \langle 2, 4 \rangle \langle 2, 4 \rangle$ 32 | 68.2% | 69.1% | 0.9% |
| | | ResNet-34 | $\langle 2, 4 \rangle \langle 2, 4 \rangle \langle 2, 4 \rangle$ 32 | 75.3% | 76.1% | 0.8% |
| | | VGG-16 | $\langle 2, 4 \rangle \langle 2, 4 \rangle \langle 2, 4 \rangle$ 32 | 70.8% | 70.9% | 0.1% |
| | | GoogleNet | $\langle 2, 4 \rangle \langle 2, 4 \rangle \langle 2, 4 \rangle$ 32 | 69.6% | 69.5% | -0.1% |

tively. The index n is omitted for simplicity and x is used to denote the original 2-dimension spatial indexes x, y .

To summarize, in the MLS format, the element-wise exponent is 2-bit instead of 5-bit, thus the **intra-group accumulation** is simplified to use 32-bit integers. On the other hand, due to the special format of group-wise scaling, $\mathcal{S}^{(p)}$ has a simple format, and the **inter-group accumulation** to calculate Z can be implemented efficiently on hardware without floating-point multiplication. Finally, the multiplication with the tensor-wise floating-point scale $S_t^{(z)}$ in Eq. 8 can usually be omitted: $S_t^{(z)}$ only needs to be multiplied with the tensor-wise floating-point scale in the following layer instead of the feature map, as long as there is no following element-wise addition on Z with another tensor.

5. Experiments

5.1. Experimental Setup

We train ResNet (He et al., 2016), VGG (Simonyan & Zisserman, 2014), and GoogleNet (Szegedy et al., 2015) on

CIFAR-10 (Krizhevsky, 2010) and ImageNet (Deng et al., 2009) with our low-bit training framework. In all the experiments, the first and the last layer are left unquantized following previous studies (Zhou et al., 2016; Mellempudi et al., 2019; Sun et al., 2019). On both CIFAR-10 and ImageNet, SGD with momentum 0.9 and weight decay $5e-4$ is used, and the initial learning rate is set to 0.1. We train the models for 90 epochs on ImageNet, and decay the learning rate by 10 every 30 epochs. On CIFAR-10, we train the models for 160 epochs and decay the learning rate by 10 at epoch 80 and 120. We experiment with the MLS tensor formats using different $\langle E_x, M_x \rangle$ configurations, the group-wise scaling are in $\langle 8, 1 \rangle$ format for all experiments in Tab. 2. And we adopt the same quantization bit-width for weight, activation and error for a simpler hardware design.

5.2. Results on CIFAR-10 and ImageNet

The training results on CIFAR-10 and ImageNet are shown in Tab. 2. We can see that our method can achieve a better balance between higher accuracy and lower bit-width.

Table 3. Accuracy of training ResNet-20 on CIFAR-10. “Div.” means that the training failed to converge. “None” means that group-wise scaling is not used ($\#group=1$).

| #group | M_g | E_x | $M_x=4$ | $M_x=3$ | $M_x=2$ | $M_x=1$ |
|--------|-------|-------|---------|---------|---------|---------|
| l | None | 0 | 90.02 | 85.68 | Div. | Div. |
| c | 0 | 0 | 91.54 | 88.35 | 82.29 | Div. |
| n | 0 | 0 | 91.78 | 89.62 | 80.71 | Div. |
| nc | 0 | 0 | 92.14 | 91.64 | 88.97 | 76.98 |
| nc | 1 | 0 | 92.37 | 91.73 | 90.39 | 82.61 |
| l | None | 0 | 90.02 | 85.68 | Div. | Div. |
| l | None | 1 | 91.67 | 90.11 | 84.72 | 70.4 |
| l | None | 2 | 92.32 | 92.34 | 91.58 | 90.32 |
| nc | 1 | 0 | 92.37 | 91.73 | 90.39 | 82.61 |
| nc | 1 | 1 | 92.52 | 92.16 | 91.48 | 89.97 |
| nc | 1 | 2 | 92.37 | 92.65 | 92.05 | 91.97 |

Previous study (Zhou et al., 2016) found that quantizing error to a low bit-width hurt the accuracy, but our method can quantize error to $M_x = 1$ on CIFAR-10, with a small accuracy drop of 0.48%, 0.55%, and 0.42% for ResNet-20, GoogleNet, and VGG-16, respectively.

On ImageNet, the accuracy degradation of our method is rather minor under 8-bit quantization (0.6% accuracy drop from 69.1% to 68.5%), which is comparable with other state-of-the-art work. In the cases with lower bit-width, our method achieves a higher accuracy (66.5%) with only 4-bit than Banner et al. (2018a) who uses 8-bit (66.4%). With $\langle 2, 4 \rangle$ data format, for all the models including ResNet-18, ResNet-34, VGG-16, and GoogleNet, our method can achieve an accuracy loss less than 1%. In this case, the bit-width of the intermediate results is $2M_x + 2^{E_x+1} - 2 = 14$, which means that the accumulation can be conducted using integers, instead of floating-points (Sun et al., 2019; Cambier et al., 2020), as we discussed in Sec. 4.2.

5.3. Ablation Studies

5.3.1. GROUP-WISE SCALING

Group-wise scaling is beneficial as the data ranges vary across different groups. We compare the average relative quantization error (ARE) of using the three grouping dimensions (Sec. 3.1) with $\langle 8, 1 \rangle$ group-wise scaling format and $\langle 0, 3 \rangle$ element format. The first row of Fig. 6 shows that the AREs are smaller when each tensor is split to $N \times C$ groups. Furthermore, we compare these grouping dimensions in the training process. The first section of Tab. 3 shows that when tensors are split to $N \times C$ groups, the training accuracy is higher. This indicates that the reduction of AREs is important for the accuracy of low-bit training. And we can see that $M_g = 1$ is important for the accuracy, especially with low M_x (e.g., when $M_x=1$, 76.98 V.S. 82.61).

Table 4. The power evaluation (mW) results of MAC units with different arithmetic, simulated by Design Compiler with TSMC 65nm process and 1GHz clock.

| Operation | MUL | LocalAcc |
|-------------------------------|-------|----------|
| Full Precision | 2.311 | 0.512 |
| 8-bit FP (Sun et al., 2019) | 0.105 | 0.512 |
| 8-bit INT (Yang et al., 2020) | 0.155 | 0.065 |
| Ours | 0.124 | 0.065 |

5.3.2. ELEMENT-WISE EXPONENT

To study the influence of the element-wise exponent, we compare the AREs of quantization with different E_x without group-wise scaling, and the results are shown in the second row of Fig. 6. Intuitively, using more exponent bits results in larger dynamic ranges and smaller AREs. And with larger E_x , the AREs of different layers are closer. Besides the ARE evaluation, Tab. 3 shows that a larger E_x achieves a better accuracy, especially when M_x is extremely small.

As shown in Fig. 6 Row 3 and Tab. 3, when jointly using the group-wise scaling and the element-wise exponent, the ARE and accuracy are further improved. And we can see that the group-wise scaling is important for simplifying the floating-point accumulator to a fixed-point one: One can use a small element-wise exponent with group-wise scaling ($\#group=nc, M_g=1, E_x=0$, Acc.=92.37%) to get a comparable accuracy to a configuration with larger $E_x=2$ without group-wise scaling (Acc.=92.32%).

5.4. Hardware Energy Consumption

Fig. 1 shows a typical convolution hardware architecture, which consists of three main components: local multiplication (MUL), local accumulation (LocalACC), and addition tree (TreeAdd). Our framework mainly improves the local multiplications and accumulations. Compared with the full-precision design, we simplify the floating-point multiplication (FP MUL) to use a bit-width less than 8 and the local floating-point (FP ACC) to use 16-bit or 32-bit integer. To evaluate the energy consumption, we implement the RTL design of the MAC unit with different arithmetic. Tab. 4 shows the hardware power results given by Design Compiler simulation with TSMC 65nm process and 1GHz clock frequency. Then, using the numbers of different operations in convolution, we can estimate our energy efficiency improvement ratio r in a 3×3 convolution as

$$r = [2.311(\#MUL) + 0.512(\#LocalACC) + 0.512(\#TreeAdd)] \div [0.124(\#MUL) + 0.065(\#LocalACC + \#GroupwiseScale) + 0.512(\#TreeAdd)] \approx 11.5 \quad (9)$$

where *GroupwiseScale* is the group-wise scaling that could be implemented efficiently as in Eq. 8. The energy

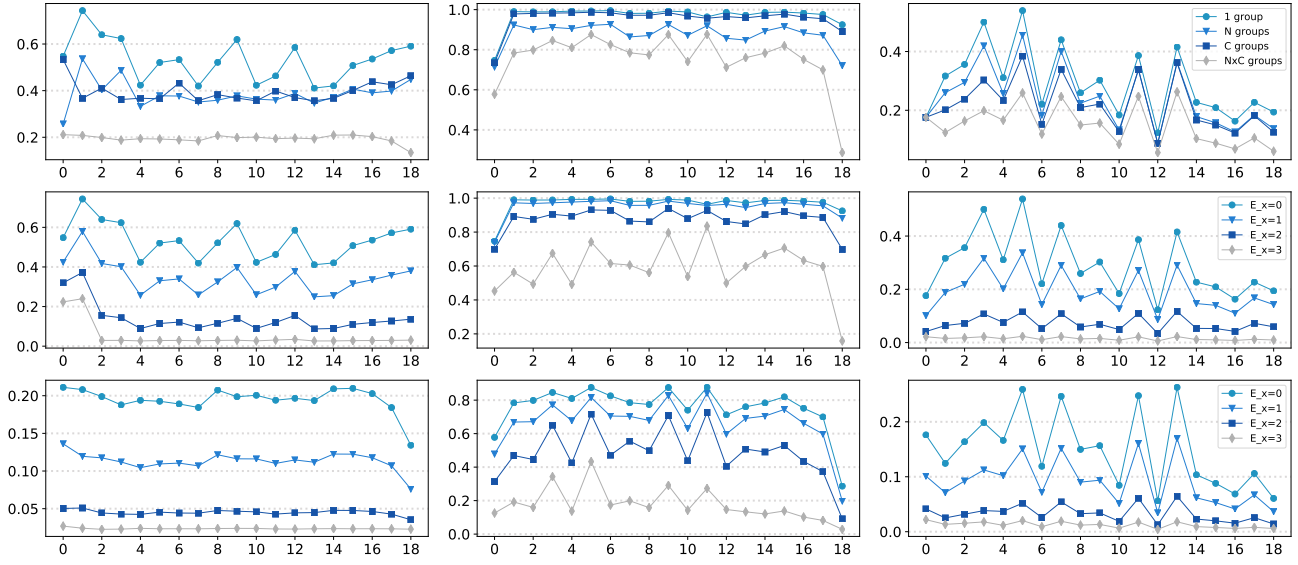


Figure 6. Average relative quantization errors (AREs) of weight, error, activation (left, middle, right) in each layer when training a ResNet-20 on CIFAR-10. X axis: Layer index. Row 1: Different grouping dimensions ($\langle 0, 3 \rangle$ formatted \bar{X} , $\langle 8, 1 \rangle$ formatted S_g); Row 2: Different E_x ($\langle E_x, 3 \rangle$ formatted \bar{X} , no group-wise scaling); Row 3: Different E_x ($\langle E_x, 3 \rangle$ formatted \bar{X} , $\langle 8, 1 \rangle$ formatted S_g , $N \times C$ groups).

estimation of 3×3 convolutions is also shown in Fig. 2.

Discussion on Overheads While our framework significantly reduces the cost of the convolution, it also introduces some overheads: 1) Group-wise maximum statistics (Line 2) and scaling factors division (Line 9) in Alg. 1 accounts for the major overhead of **dynamic quantization**. The cost of these two operations is comparable with that of a batch normalization operation, since they are calculated by similar formulas on the same amount of values. And as shown in Tab. 1, the number of multiplication and addition operation in batch normalization is orders of magnitude smaller than that in the convolutions. Hence, the energy consumption of batch normalization and dynamic quantization is relatively smaller compared with convolution (refer to the appendix for the detailed energy estimation). 2) The **group-wise scaling factors** introduce additional scaling. Fortunately, when using the $\langle E_g, 0 \rangle$ or $\langle E_g, 1 \rangle$ format, we can implement the group-wise scaling efficiently with shifting (Eq. 3). And the energy consumption is comparable to a LocalACC operation. We have already taken this overhead into account when estimating the energy efficiency improvement ratio of convolution in Eq. 9.

To summarize, the introduced overhead of our framework is low compared with the reduced cost. Taking the two aforementioned overheads into consideration, we can estimate that our whole low-bit training framework could achieve $8.3 \sim 10.2\times$ higher energy efficiency than the

full-precision framework when training different models on ImageNet. Compared with previous low-bit floating-point training frameworks (Sun et al., 2019), our framework can achieve $1.9 \sim 2.3\times$ higher energy efficiency due to the simplified integer accumulator. For completeness, the detailed energy estimation of different operation types when training ResNet-34 on ImageNet is shown in the appendix.

6. Conclusion

This paper proposes a low-bit training framework to enable training CNNs with lower bit-width convolution while retaining the accuracy. Specifically, we design a multi-level scaling (MLS) tensor format, and develop the corresponding quantization procedure and low-bit convolution arithmetic. Experimental results and the energy consumption simulation of the computing unit demonstrate the effectiveness of our framework. Compared with previous low-bit integer training frameworks, our framework can retain a higher accuracy for a variety of models. Compared with previous low-bit floating-point training frameworks, our framework can achieve much higher energy efficiency.

References

- Abadi, M., Agarwal, A., Barham, P., Brevdo, E., Chen, Z., Citro, C., Corrado, G. S., Davis, A., Dean, J., Devin, M., Ghemawat, S., Goodfellow, I. J., Harp, A., Irving, G., Isard, M., Jia, Y., Józefowicz, R., Kaiser, L., Kudlur, M., Levenberg, J., Mané, D., Monga, R., Moore, S., Murray, D., Olah, C., Schuster, M., Shlens, J., Steiner, B., Sutskever, I., Talwar, K., Tucker, P., Vanhoucke, V., Vasudevan, V., Viégas, F., Vinyals, O., Warden, P., Wattemberg, M., Wicke, M., Yu, Y., and Zheng, X. Tensorflow: Large-scale machine learning on heterogeneous distributed systems. *ArXiv*, abs/1603.04467, 2016.
- Banner, R., Hubara, I., Hoffer, E., and Soudry, D. Scalable methods for 8-bit training of neural networks. In *NeurIPS*, 2018a.
- Banner, R., Nahshan, Y., and Soudry, D. Post training 4-bit quantization of convolutional networks for rapid-deployment. In *NeurIPS*, 2018b.
- Cambier, L., Bhiwandiwalla, A., Gong, T., Nekui, M., Elilbol, O. H., and Tang, H. Shifted and squeezed 8-bit floating point format for low-precision training of deep neural networks. *ArXiv*, abs/2001.05674, 2020.
- Das, D., Mellempudi, N., Mudigere, D., Kalamkar, D., Avancha, S., Banerjee, K., Sridharan, S., Vaidyanathan, K., Kaul, B., Georganas, E., Heinecke, A., Dubey, P., Corbal, J., Shustrov, N., Dubtsov, R., Fomenko, E., and Pirogov, V. O. Mixed precision training of convolutional neural networks using integer operations. *ArXiv*, abs/1802.00930, 2018.
- Deng, J., Dong, W., Socher, R., Li, L.-J., Li, K., and Fei-Fei, L. Imagenet: A large-scale hierarchical image database. In *2009 IEEE conference on computer vision and pattern recognition*, pp. 248–255. Ieee, 2009.
- Dong, Z., Yao, Z., Gholami, A., Mahoney, M., and Keutzer, K. Hawq: Hessian aware quantization of neural networks with mixed-precision. *ArXiv*, abs/1905.03696, 2019.
- Gupta, S., Agrawal, A., Gopalakrishnan, K., and Narayanan, P. Deep learning with limited numerical precision. In *ICML*, 2015.
- Gysel, P., Pimentel, J. J., Motamedi, M., and Ghiasi, S. Ristretto: A framework for empirical study of resource-efficient inference in convolutional neural networks. *IEEE Transactions on Neural Networks and Learning Systems*, 29:5784–5789, 2018.
- He, K., Zhang, X., Ren, S., and Sun, J. Deep residual learning for image recognition. In *Proceedings of the IEEE conference on computer vision and pattern recognition*, pp. 770–778, 2016.
- Horowitz, M. 1.1 computing’s energy problem (and what we can do about it). *2014 IEEE International Solid-State Circuits Conference Digest of Technical Papers (ISSCC)*, pp. 10–14, 2014.
- Hough, D. G. The ieee standard 754: One for the history books. *Computer*, 52(12):109–112, 2019.
- Jacob, B., Kligys, S., Chen, B., Zhu, M., Tang, M., Howard, A. G., Adam, H., and Kalenichenko, D. Quantization and training of neural networks for efficient integer-arithmetic-only inference. *2018 IEEE/CVF Conference on Computer Vision and Pattern Recognition*, pp. 2704–2713, 2018.
- Jacob, P. W. et al. gemmlowp: a small self-contained low-precision gemm library.(2017). [OL], 2017. <https://github.com/google/gemmlowp> Accessed February 1, 2021.
- Köster, U., Webb, T., Wang, X., Nassar, M., Bansal, A. K., Constable, W., Elilbol, O., Hall, S., Hornof, L., Khosrowshahi, A., Kloss, C., Pai, R. J., and Rao, N. Flexpoint: An adaptive numerical format for efficient training of deep neural networks. In *NIPS*, 2017.
- Krizhevsky, A. Convolutional deep belief networks on cifar-10. 2010.
- Krizhevsky, A., Sutskever, I., and Hinton, G. E. Imagenet classification with deep convolutional neural networks. In Pereira, F., Burges, C. J. C., Bottou, L., and Weinberger, K. Q. (eds.), *Advances in Neural Information Processing Systems 25*, pp. 1097–1105. Curran Associates, Inc., 2012.
- Li, F., Zhang, B., and Liu, B. Ternary weight networks. *arXiv preprint arXiv:1605.04711*, 2016.
- Lin, D. D., Talathi, S. S., and Annapureddy, V. S. Fixed point quantization of deep convolutional networks. *ArXiv*, abs/1511.06393, 2015.
- Liu, W., Anguelov, D., Erhan, D., Szegedy, C., Reed, S., Fu, C.-Y., and Berg, A. C. Ssd: Single shot multibox detector. In *European conference on computer vision*, pp. 21–37. Springer, 2016.
- Liu, Z., Shen, Z., Savvides, M., and Cheng, K. Reactnet: Towards precise binary neural network with generalized activation functions. *ArXiv*, abs/2003.03488, 2020.
- Mellempudi, N., Srinivasan, S., Das, D., and Kaul, B. Mixed precision training with 8-bit floating point. *ArXiv*, abs/1905.12334, 2019.
- Park, E., Ahn, J., and Yoo, S. Weighted-entropy-based quantization for deep neural networks. *2017 IEEE Conference*

on *Computer Vision and Pattern Recognition (CVPR)*, pp. 7197–7205, 2017.

Qin, H., Gong, R., Liu, X., Wei, Z., Yu, F., and Song, J. Ir-net: Forward and backward information retention for highly accurate binary neural networks. *ArXiv*, abs/1909.10788, 2019.

Rastegari, M., Ordonez, V., Redmon, J., and Farhadi, A. Xnor-net: Imagenet classification using binary convolutional neural networks. In *ECCV*, 2016.

Redmon, J., Divvala, S., Girshick, R., and Farhadi, A. You only look once: Unified, real-time object detection. In *Proceedings of the IEEE conference on computer vision and pattern recognition*, pp. 779–788, 2016.

Simonyan, K. and Zisserman, A. Very deep convolutional networks for large-scale image recognition. *arXiv preprint arXiv:1409.1556*, 2014.

Sun, X., Choi, J., Chen, C.-Y., Wang, N., Venkataramani, S., Srinivasan, V., Cui, X., Zhang, W., and Gopalakrishnan, K. Hybrid 8-bit floating point (hfp8) training and inference for deep neural networks. In *NeurIPS*, 2019.

Szegedy, C., Liu, W., Jia, Y., Sermanet, P., Reed, S., Anguelov, D., Erhan, D., Vanhoucke, V., and Rabinovich, A. Going deeper with convolutions. *2015 IEEE Conference on Computer Vision and Pattern Recognition (CVPR)*, pp. 1–9, 2015.

Wang, N., Choi, J., Brand, D., Chen, C.-Y., and Gopalakrishnan, K. Training deep neural networks with 8-bit floating point numbers. In *NeurIPS*, 2018.

Wu, S., Li, G., Chen, F., and Shi, L. Training and inference with integers in deep neural networks. *ArXiv*, abs/1802.04680, 2018.

Yang, Y., Wu, S., Deng, L., Yan, T., Xie, Y., and Li, G. Training high-performance and large-scale deep neural networks with full 8-bit integers. *Neural networks : the official journal of the International Neural Network Society*, 125:70–82, 2020.

Zhou, S., Ni, Z., Zhou, X., Wen, H., Wu, Y., and Zou, Y. Dorefa-net: Training low bitwidth convolutional neural networks with low bitwidth gradients. *ArXiv*, abs/1606.06160, 2016.

A. Low-bit Training Framework

Algorithm 2 The low-bit training framework

Input: L : number of layers; $W_t^{1:L}$: float weights; A^0 : inputs; T : label; lr : learning rate
Output: $W_{t+1}^{1:L}$: updated float weights for the next step $t + 1$

```

/* forward propagation */
for  $l$  in  $1 : L$  do
     $qW^l = \text{DynamicQuantization}(W^l)$ 
     $qA^{l-1} = \text{DynamicQuantization}(A^{l-1})$ 
     $Z^l = \text{LowbitConv}(qW^l, qA^{l-1})$ 
     $Y^l = \text{BatchNorm}(Z^l)$ 
     $A^l = \text{Activation}(Y^l)$ 
end
 $\frac{\partial \text{loss}}{\partial A^l} = \text{Criterion}(A^L, T)$ 

/* backward propagation */
for  $l$  in  $L : 1$  do
     $\frac{\partial \text{loss}}{\partial Y^l} = \frac{\partial \text{loss}}{\partial A^l} \times \text{Activation}'(Y^l)$ 
     $\frac{\partial \text{loss}}{\partial Z^l} = \frac{\partial \text{loss}}{\partial Y^l} \times \frac{\partial Y^l}{\partial Z^l}$ 
     $qE^l = \text{DynamicQuantization}(\frac{\partial \text{loss}}{\partial Z^l})$ 
     $G^l = \text{LowbitConv}(qE^l, qA^{l-1})$ 
     $W_{t+1}^l = W^l - lr \times G^l$ 
    if  $l$  is not 1 then
         $\frac{\partial \text{loss}}{\partial qA^{l-1}} = \text{LowbitConv}(qE^l, qW^l)$ 
         $\frac{\partial \text{loss}}{\partial A^{l-1}} = \text{STE}(\frac{\partial \text{loss}}{\partial qA^{l-1}})$ 
    end
end
Return  $W_{t+1}^{1:L}$ 

```

A training iteration in our low-bit training framework is summarized in Alg. 2. In the backward propagation, the update formula is of the vanilla stochastic gradient descent (SGD) for clarity, whereas in practice, one can use other optimizers such as SGD with momentum. The t subscripts denoting the time step t are all omitted for simplicity.

B. Accumulation Bit-width

Convolution consists of multiplication and accumulation. When different data formats are used, the results of multiplication have different dynamic ranges.

As specified by the IEEE 754 standard, the gradual underflow behavior of a floating-point representation that has M -bit mantissa (Man) and E -bit exponent (Exp) is as follows. If Exp is not equal to the minimum value, the float value is not underflow, and is calculated as

$$\begin{aligned} float &= \text{Frac} \times 2^{-Exp} \\ &= \left(1 + \frac{Man}{2^M}\right) \times 2^{-Exp}. \end{aligned} \quad (10)$$

If Exp is equal to the minimum value, the float value is an gradual-underflowed value, and is calculated as

$$\begin{aligned} float &= \text{Frac} \times 2^{-Exp} \\ &= \left(0 + \frac{Man}{2^M}\right) \times 2^{-Exp}, \end{aligned} \quad (11)$$

where Frac is $(M + 1)$ -bit fraction, calculated by adding a 0 or 1 at the highest bit of mantissa.

As discussed in Sec. 4.2 in the paper, we calculate the product of two numbers as

$$\begin{aligned} float_1 \times float_2 &= \text{Frac}_1 \times 2^{-Exp_1} \times \text{Frac}_2 \times 2^{-Exp_2} \\ &= (\text{Frac}_1 \times \text{Frac}_2) \times 2^{-Exp_1 - Exp_2}, \end{aligned} \quad (12)$$

where $\text{Frac}_1 \times \text{Frac}_2$ is a $(M + 1)$ -bit multiplication, and the result is $(2M + 2)$ -bit. Since the minimum value of exponent is used to represent underflow, E -bit Exp represents $2^E - 1$ levels and “ $\times 2^{-Exp}$ ” is $(2^E - 2)$ -bit shifting. Therefore, “ $\times 2^{-Exp_1 - Exp_2}$ ” is $(2^{E+1} - 4)$ -bit shifting, and the final result of floating-point multiplication has a dynamic range of $2M + 2 + 2^{E+1} - 4 = (2M + 2^E - 2)$ -bit. These resulting $(2M + 2^{E+1} - 2)$ -bit integer values need to be accumulated with enough bit-width to get the partial sum. In previous 8-bit floating-point frameworks, the accumulator has to be floating-point since they use $E = 5$. In contrast, we can use a 32-bit integer accumulator, since we adopt $E = 2, M = 4, (2M + 2^{E+1} - 2) = 14$ in the MLS tensor format on ImageNet.

C. Energy Estimation

For completeness, we give the detailed energy estimation of different operation types when training ResNet-34 on ImageNet in Tab. 5. The energy consumption is calculated by multiplying the operation amount (Tab. 1 in the original paper) and the energy consumption of each operation (Tab. 4 in the original paper).

Considering a convolution with C_i input channels, C_o output channels, $K \times K$ kernel size, and $W \times H$ feature map size, the operation amounts of floating-point multiplications and additions are $C_i \times C_o \times K \times K \times W \times H$, and the operation amount in the whole network is calculated by accumulating the operation amounts of each layer in both the forward and backward processes. In our low-bit training framework, floating-point additions are only reserved in the adder tree, and the amount is $C_i \times C_o \times W \times H$. The amount of integer accumulation is equal to the other local addition and shifting (which is the same as the adder tree).

For dynamic quantization, we consider that 4 multiplications and 2 additions are needed for one element: one addition is to calculate the max (Alg. 1 Line 2 in the original paper) and

Table 5. The comparison of the detailed energy estimation of training ResNet-34 on ImageNet using full-precision training and our low-bit training framework. “DQ” means dynamic quantization, which is an additional operation in our framework.

| Op Name | Full Precision Training | | | Our Low-Bit Training | | |
|------------|-------------------------|-----------|-----------------|----------------------|-------------------|-----------------|
| | Op Type | Op Amount | Energy/ μ J | Op Type | Op Amount | Energy/ μ J |
| Conv | FloatMul | 1.12E+10 | 25900 | FP7Mul | 1.12E+10 | 1390 |
| | FloatAdd | 1.12E+10 | 5740 | IntAdd | 1.12E+10 | 729 |
| | - | 0 | 0 | FloatAdd | 1.21E+09 | 620 |
| BN | FloatMul | 4.87E+07 | 101 | FloatMul | 4.87E+07 | 101 |
| | FloatAdd | 4.38E+07 | 24.9 | FloatAdd | 4.38E+07 | 24.9 |
| FC | FloatMul | 3.07E+06 | 7.1 | FloatMul | 3.07E+06 | 7.1 |
| | FloatAdd | 3.07E+06 | 1.57 | FloatAdd | 3.07E+06 | 1.57 |
| SGD Update | FloatMul | 5.16E+07 | 119 | FloatMul | 5.16E+07 | 119 |
| | FloatAdd | 5.16E+07 | 26.4 | FloatAdd | 5.16E+07 | 26.4 |
| DQ | - | 0 | 0 | FloatMul | 3.90E+7 + 6.88E+7 | 249 |
| | - | 0 | 0 | FloatAdd | 1.95E+6 + 3.44E+7 | 27.6 |
| EW-Add | FloatAdd | 2.88E+06 | 1.47 | FloatAdd | 2.88E+06 | 1.47 |
| | - | 0 | 0 | FloatMul | 2.88E+06 | 6.66 |
| Sum | | | 32000 | | | 3130 |

the other one is to calculate the sum of $Frac_{xs}$ and R (Alg. 1 Line 13 in the original paper), and the four multiplications are used for the Alg. 1 Line 4 and Line 9 in the original paper. Note that other multiplications and divisions in Alg. 1 describe the simulation of the dynamic quantization process on the floating-point platform, and they do not actually introduce overhead. The number of elements is $C \times W \times H$ for activation and error, and $C_i \times C_o \times K \times K$ for weight, and their energy consumption are shown separately in Tab. 5.

As for batch normalization, fully connected layer, SGD update, the operation amount and energy consumption are the same for both the full-precision and our low-bit training framework. Specifically, 9 multiplications and 10 additions are performed on each element of a $C \times W \times H$ feature map in the forward and backward processes for batch normalization. The forward process of batch normalization is:

$$\begin{aligned}
 \mu &= \frac{1}{M} \sum_{i=1}^M x_i \\
 \sigma^2 &= \frac{1}{M} \sum_{i=1}^M x_i^2 - \mu^2 \\
 y_i &= \frac{x_i - \mu}{\sqrt{\sigma^2 + 0.00005}} \\
 z_i &= \gamma y_i + \beta.
 \end{aligned} \tag{13}$$

We can see that in the forward process of batch normalization, one addition is used by one element to calculate the batch mean, and one multiplication and one addition

are used to calculate the batch variance, and two multiplications and two additions are used for normalization and affine transformation.

The backward process of batch normalization is:

$$\begin{aligned}
 \frac{\partial L}{\partial \gamma} &= \sum_{i=1}^M \frac{\partial L}{\partial z_i} \cdot y_i \\
 \frac{\partial L}{\partial \beta} &= \sum_{i=1}^M \frac{\partial L}{\partial z_i} \\
 \frac{\partial L}{\partial y_i} &= \frac{\partial L}{\partial z_i} \cdot \gamma \\
 t_1 &= \sum_{j=1}^M \frac{\partial L}{\partial y_j} \\
 t_2 &= \sum_{j=1}^M \left(\frac{\partial L}{\partial y_j} \cdot y_j \right) \\
 \frac{\partial L}{\partial x_i} &= \frac{M \frac{\partial L}{\partial y_i} - t_1 - y_i \cdot t_2}{M \cdot \sqrt{\sigma^2 + 0.00005}}.
 \end{aligned} \tag{14}$$

There are six multiplications and six additions performed on one element in the backward process of batch normalization (“1M1A, 1A, 1M, 1A, 1M1A, 3M2A” for each formula in Eq. 14, respectively).

For element-wise addition of two MLS tensors z_1, z_2 , we need to multiply the ratio of their tensor-wise scales $S_t^{z_1}/S_t^{z_2}$ to Z_2 , and then the element-wise addition can be conducted. Therefore, extra multiplications of the same

amount are needed in our low-bit training framework.

The last row of Tab. 5 shows the sum of the energy consumption of previous operations, and the results are not exactly the sum of the numbers in previous rows. The results show that our low-bit training framework achieves $32000 \div 3130 = 10.2\times$ higher energy efficiency than full-precision training. The energy consumption calculation of other networks and 8-bit floating-point training can be conducted similarly as the above analysis, and is not discussed here.